Macromolecules

Article

pubs.acs.org/Macromolecules

# Alcohol-Soluble n-Type Conjugated Polyelectrolyte as Electron Transport Layer for Polymer Solar Cells

Lin Hu,[†] Feiyan Wu,[†] Chunquan Li,[§] Aifeng Hu,[†] Xiaotian Hu,[†] Yong Zhang,[†] Lie Chen,*[,†,‡] and Yiwang Chen[†,‡]

[†]College of Chemistry/Institute of Polymers, [‡]Jiangxi Provincial Key Laboratory of New Energy Chemistry, and [§]Department of Electronic Information Engineering, Nanchang University, 999 Xuefu Avenue, Nanchang 330031, China

Supporting Information

**ABSTRACT:** A novel alcohol-soluble n-type conjugated polyelectrolyte (n-CPE) poly-2,5-bis(2-octyldodecyl)-3,6-bis(thiophen-2-yl)-pyrrolo[3,4-*c*]pyrrole-1,4-dione-*alt*-2,5-bis[6-(*N*,*N*,*N*-trimethylammonium)hexyl]-3,6-bis(thiophen-2-yl)-pyrrolo[3,4-*c*]pyrrole-1,4-dione (PDPPNBr) is synthesized for applications as an electron transport layer (ETL) in an inverted polymer solar cells (PSCs) device. Because of the electron-deficient nature of diketopyrrolopyrrole (DPP) backbone and its planar structure, PDPPNBr is endowed with high conductivity and electron mobility. The interfacial dipole moment created by n-CPE PDPPNBr can substantially reduce the work function of ITO and induce a better energy alignment in the device, facilitating electron extraction and decreasing exctions recombination at active layer/cathode interface. As a result, the power conversion efficiency (PCE) of the inverted devices based poly(3-hexylthiophene) (P3HT):(6,6)-phenyl-$C_{61}$ butyric acid methyl ester ($PC_{61}BM$) active layer with PDPPNBr as ETL achieves a value of 4.03%, with 25% improvement than that of the control device with ZnO ETL. Moreover, the universal PDPPNBr ETL also delivers a notable PCE of 8.02% in the devices based on polythieno[3,4-*b*]-thiophene-*co*-benzodithiophene (PTB7):(6,6)-phenyl-$C_{71}$-butyric acid methyl ester ($PC_{71}BM$). To our best knowledge, this is the first time that n-type conjugated polyelectrolyte-based cathode interlayer is reported. Quite different from the traditional p-type conjugated and nonconjugated polyelectrolytes ETLs, n-CPE PDPPNBr as ETL could function efficiently with a thickness approximate 30 nm because of the high conductivity and electron mobility. Furthermore, the PDPPNBr interlayer also can ensure the device with the improved long-term stability. The successful application of this alcohol solution processed n-type conjugated polyelectrolyte indicates that the electron-deficient planar structure with high electron mobility could be very promising in developing high performance and environmentally friendly polymer solar cells.

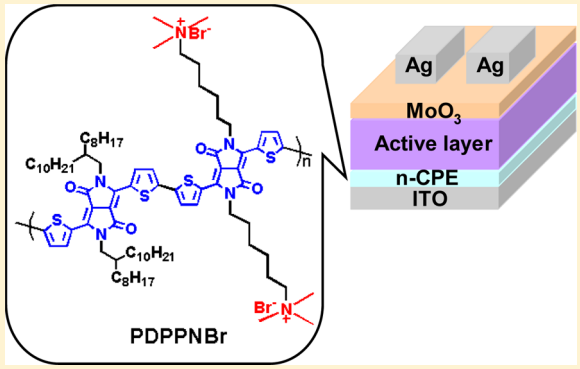


## 1. INTRODUCTION

Bulk heterojunction (BHJ) polymer cells (PSCs) have achieved tremendous progress in the past decade due to their advantages such as low-cost manufacturing, mechanical flexibility, and easy fabrication for large-scale production.[1−5] Recently, the power conversion efficiencies (PCE) of the state-of-the-art devices have already exceeded 10%.[6−11] Especially, the so-called inverted structure PSCs are of particular interest for the superior efficiency and stability compared with the conventional devices.[12−14] For the inverted PSCs, the BHJ active layer is coated between the bottom cathode of indium tin oxide (ITO) and top anode of a high work function (WF) metal (Ag or Au).[15,16] To obtain a more brilliant performance, the most common and successful strategy is developing an original photoactive layer material and fabricating a desirable device structure. Nevertheless, the interface engineering in the device also plays a significant role for a breakup in the superior efficiency and stability. An excellent interlayer can not only build a tunable energy level alignment between the contact interface to facilitate the charge extraction and transportation but also promote interfacial stability for a high-efficiency and stable device eventually.[17,18] In the inverted devices, the inorganic metal oxides such as titanium oxide ($TiO_x$) or zinc oxide (ZnO) have always been incorporated as cathode interlayers or electron transport layers (ETLs) to modify ITO cathode due to their high charge mobility and electron selective properties.[19,20] However, these inorganic ETLs are not well compatible with the organic active layer. Moreover, most of them typically require a high-temperature annealing process to yield high charge carrier mobility, which do not meet with the high throughput roll-to-roll manufacturing techniques for commercial application.

In order to overcome the weakness of the inorganic metal oxides, a series of organic interlayer materials have already been explored, including small molecule-based organic interlayers and

**Received:** May 27, 2015
**Revised:** August 2, 2015





DOI: 10.1021/acs.macromol.5b01137
*Macromolecules* XXXX, XXX, XXX−XXX

**Scheme 1. Synthesis Routes of the Copolymer PDPPBr and n-CPE PDPPNBr**[a]

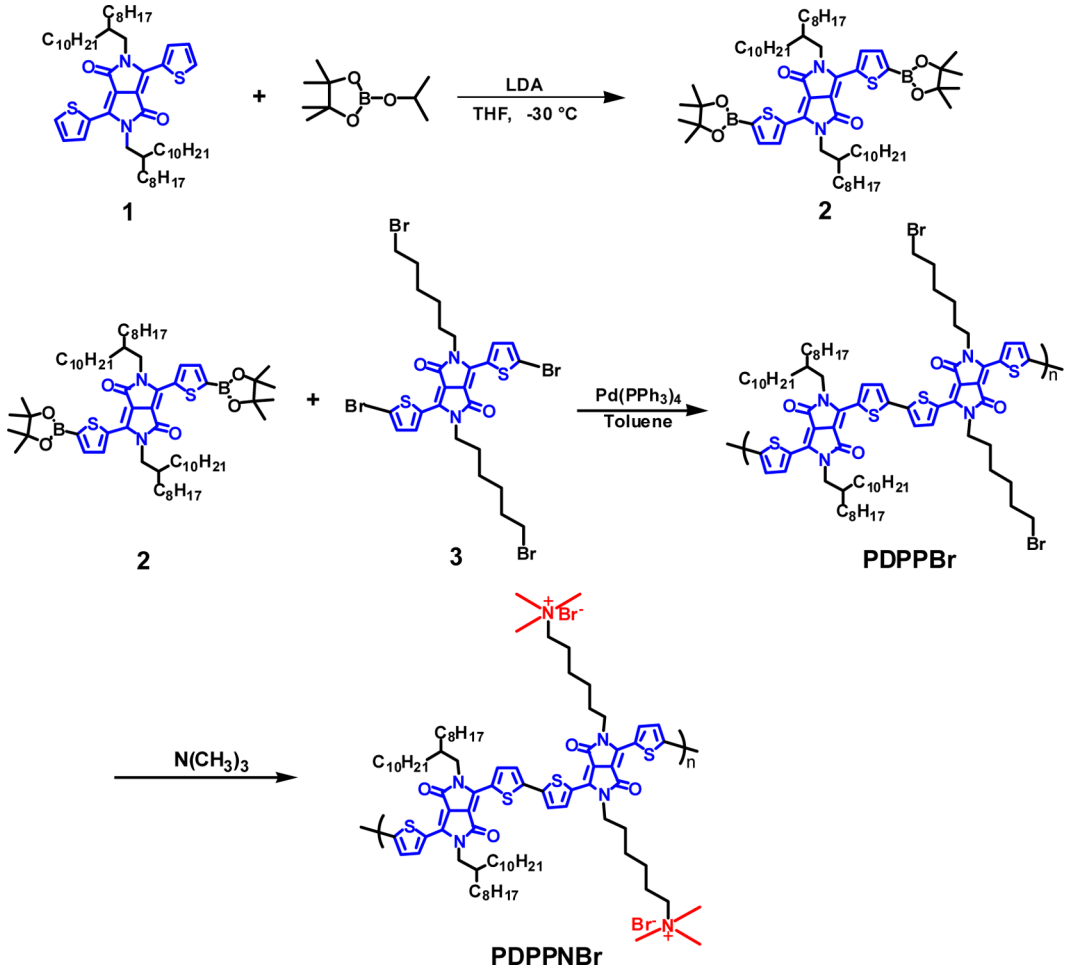


[a]The inset is the photographs of the copolymer PDPPBr and n-CPE PDPPNBr dissolved in methanol solution.

polymer-based organic interlayers. The successful small-molecular interlayers are the fullerene derivatives, perylenediimide salt, and so on.[21,22] However, it is limited due to the difficulty of product purification and an unfavorable film of the interlayer. The typical polymer-based interlayers are mainly polyelectrolytes (PEs), such as poly [(9,9-bis(3′-(*N*,*N*-dimethylamino)propyl)-2,7- fluorene)-*alt*-2,7-(9,9-dioctylfluorene (PFN) and polyethylenimine ethoxylated (PEIE), which have been paid more attention for the reasons of good film forming properties and easy to preparation.[11,23−25] It has been reported the PEs were introduced as interlayers to afford remarkable performance improvement in the PSCs, and the power conversion has broken through 10%.[26] The ionic or polar pendant groups of the PEs side chain render the conjugated polymers soluble in water, methanol, dimethylformamide, and other polar solvents, which can efficiently avoid the erosion from the active layer dissolved in the chlorinated solvents. More importantly, the different polar groups in these PEs can form a strong interfacial dipole moments in the cathode interface, resulting in a shift of the vacuum level at the PE/cathode interface and an adjusted work function of cathode electrodes (such as Cu, Ag, and Au). Therefore, electron transport and injection from the active layer to the cathode can be effectively regulated.[27,28] However, the present research about the PEs mainly focuses on the pendent polar groups but neglects the influence of PEs backbone on the characteristics of the interlayer materials. What is more, most of reported PEs are based on p-type conjugated or nonconjugated polymer backbones, such as polythiophenes, polyfluorenes, polycarbazoles, and polyethylenimine.[29−32] Theoretically, these p-type conjugated or nonconjugate backbone as ETLs would hamper the electron extraction and transportation, so that the thickness of these PEs interlayers is extremely limited to only a few nanometers (usually less than 10 nm),[33] which is not helpful to high throughput commercial application in the near future. Although metal-containing conjugated polymers interlayer, e.g. PFEN-Hg, with a thickness ∼20 nm demonstrated a good device performance, the toxic metal Hg has been incorporated.[34]

In this study, we concentrate in the PEs backbone to design and synthesize a novel n-type conjugated polyelectrolyte (n-CPE) poly-2,5-bis(2-octyldodecyl)-3,6-bis(thiophen-2-yl)-pyrrolo[3,4-*c*]pyrrole-1,4-dione-*alt*-2,5-bis-[6-(*N*,*N*,*N*-trimethylammonium)hexyl]-3,6-bis(thiophen-2-yl)-pyrrolo-[3,4-*c*]pyrrole-1,4-dione (PDPPNBr) (Scheme 1). We find that the feature of the conjugated backbone of the polyelectrolyte has a significant impact on the properties. Because of the electron-deficient nature and strong interactions of diketopyrrolopyrrole (DPP) backbone, this novel n-CPE shows high conductivity and electron mobility.[35] Moreover, the introduced ammonium salt polar pendant groups in the n-CPE PDPPNBr can not only create favorable dipole moments to provide better energy alignment in solar cells but also endow n-CPE PDPPNBr with


DOI: 10.1021/acs.macromol.5b01137
*Macromolecules* XXXX, XXX, XXX−XXX

good solubility in methanol and other environmentally friendly solvents. Subsequently, the n-CPE PDPPNBr as ETL has been successfully applied in the inverted device with a structure of ITO/n-CPE/P3HT:$PC_{61}BM$/$MoO_3$/Ag, and a desirable PCE of 4.03% is obtained, which is about 24% enhancement than the value obtained from the control device with ZnO ETL. Replacing the active layer with the low-bandgap donor polythieno[3,4-*b*]-thiophene-*co*-benzodithiophene (PTB7) and acceptor [6,6]-phenyl-$C_{71}$-butyric acid methyl ester ($PC_{71}BM$), a prominent PCE as high as 8.02% is achieved. It is worthy to note that this is the first time that n-type conjugated polyelectrolyte-based interlayer is reported. Inspiringly, quite different from p-type conjugated or nonconjugated PEs, the high electron mobility and conductivity benefitted from the n-type feature and solid-state packing can effectively alleviate the thickness limitation and make PDPPNBr capable of functioning efficiently in a wide thickness range of 6 to ∼30 nm. This characteristic of the solution processed n-CPE ETL provides the feasibility of large-area roll-to-roll manufacturing techniques. Additionally, the PDPPNBr interlayer also can ensure the device with an improved long-term stability. These findings indicate this unprecedented alcohol-soluble n-type CPE could be a desirable candidate for the interfacial layer materials in highly efficient and stable PSCs.

## 2. RESULTS AND DISCUSSION

The synthesis and structure of the n-type conjugated polyelectrolyte PDPPNBr are shown in Scheme 1 (synthesis details are provided in the Supporting Information). Compound **1** reacted with 2-isopropoxy-4,4,5,5-tetramethyl-1,3,2-dioxoborolane to afford DPP-based compound **2**. Then, the copolymer PDPPBr was first prepared by the Suzuki coupling polymerization between compounds **2** and **3**. The copolymer PDPPBr was purified by precipitation in methanol followed by Soxhlet extraction using methanol, acetone, and chloroform. The final dark-purple solid was easily soluble in the common organic solvents such as chloroform, chlorobenzene, and toluene at room temperature. The ionized copolymer PDPPNBr was obtained through an almost quantitative quaternization by treating the copolymer with a trimethylamine in tetrahydrofuran (THF) solutions at low temperature.[24,36] Because of the existence of the ammonium salt polar pendant groups, the resulted n-CPE PDPPNBr can be readily dissolved in polar solvents including methanol, dimethylformamide (DMF), and dimethyl sulfoxide (DMSO). The comparison photographs of the copolymer PDPPBr and its corresponding n-CPE PDPPNBr dissolved in methanol solution are shown in Figure 1. It can be observed that the copolymer PDPPBr presents a large amount of precipitate at the bottom of the bottle, while the n-CPE PDPPNBr shows a clearly blue methanol solution, thanks to the ammonium salt polar groups. In addition, all the intermediates and final product have been thoroughly purified, and the chemical structures of the products were characterized by spectroscopic methods, from which satisfactory analysis data were obtained (for the corresponding $^1H$ NMR and $^{13}C$ NMR of the intermediates and final product see the Experimental Section in Figures S1−S3 of the Supporting Information).

The ultraviolet−visible (UV−vis) absorption spectra of the copolymer PDPPBr and the conjugated polyelectrolyte PDPPNBr in solution and solid states are shown in Figure 1. Owing to the same backbone of PDPPBr and PDPPNBr, the copolymer and conjugated polyelectrolyte solutions maintain similar absorption bands. However, the maximum absorption wavelength ($\lambda_{max}$) of both thin films displays an obvious red-shift

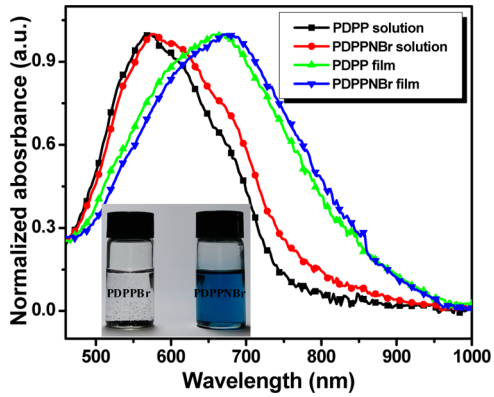


**Figure 1.** UV−vis absorption spectra of PDPPBr in chloroform solution and PDPPNBr in methyl alcohol solution as well as the corresponding thin films.

(∼150 nm) relative to that of their corresponding solutions, resulting from intermolecular interactions of the diketopyrrolopyrrole backbone favoring the strong solid-state packing. The frontier molecular orbital energy of copolymer PDPPBr and the conjugated polyelectrolyte PDPPNBr was calculated from the cyclic voltammetry (CV), which is presented in Figure S4. Based on the reduction potential (−0.78 eV) and the oxidation potential (0.75 eV), the lowest unoccupied molecular orbital (LUMO) and the highest occupied molecular orbital (HOMO) of PDPPNBr are estimated to be −3.62 and −5.15 eV, respectively. The physiochemical properties of the copolymer are summarized in Table S1. The energy levels are well consistent with density functional theory (DFT) calculations with the Gaussian 09 at the B3LYP/6-31g(d) level for copolymer PDPPBr, as shown in Figure S5. After optimizing the geometrical structures with a fixed repeating structure, the calculated HOMO and LUMO energy levels are −4.89 and −2.96 eV, respectively. Furthermore, the torsion angle between the two thiophene rings is only 6° tilted from the planar geometry, which would be in favor of the charge transfer.[37,38]

The polar side chain in the polyelectrolyte is preferable to form an aligned dipole moment at metal/organic material interface, which can modify the work function (WF) of the electrode by inducing a vacuum-level shift.[39] To characterize the WF change of PDPPNBr-modified ITO electrode, ultraviolet photoelectron spectroscopy (UPS) was carried out. A thin layer of PDPPNBr with a thickness of approximately 12 nm was deposited on the ITO substrate. As shown in Figure 2a, the bare ITO exhibits a typical WF value of 4.84 eV, in accordance with the literature,[17] while the WF moves to 4.12 eV by 0.72 eV shift when ITO is modified with PDPPNBr. Upon deposition of PDPPNBr on ITO, the negative bromide counterions tend to be located near the hydrophilic ITO, whereas the hydrophobic conjugated polymer backbone preferentially locates on the surface (as shown schematically in Figure 2b),[39,40] which would spontaneously give rise to the formation of interfacial dipole at the ITO/PDPPNBr interface. The dipole moment pointing away from the ITO surface to active layer makes the substantial reduction of WF through the swift down of the vacuum level ($E_{vac}$) of the substrates closer to that of the active layer. Consequently, the interfacial dipole formation at ITO/PDPPNBr interface can lower the Schottky barrier and favor a better energy alignment to facilitate the electron injection and transport from the photo-harvest layer to ITO.


DOI: 10.1021/acs.macromol.5b01137
*Macromolecules* XXXX, XXX, XXX−XXX

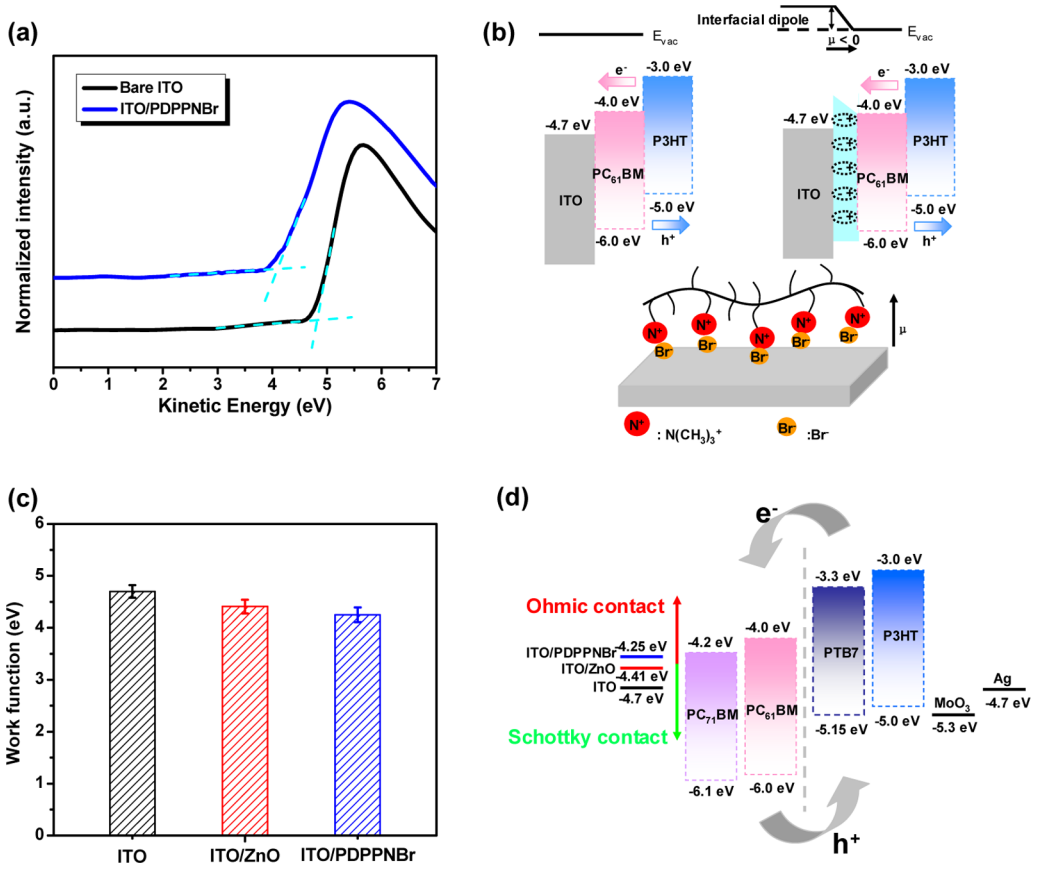


**Figure 2.** (a) Work function of the bare ITO and PDPPNBr modified ITO by ultraviolet photoelectron spectroscopy (UPS). (b) Schematic of the schematically proposal formation of interfacial dipole at ITO/PDPPNBr interface in the inverted devices. (c) Work function error graph of the bare ITO and ITO coated with ZnO and PDPPNBr, respectively. (d) Schematic energy level diagram of the different investigated electrode interlayers in various photoactive layer devices.

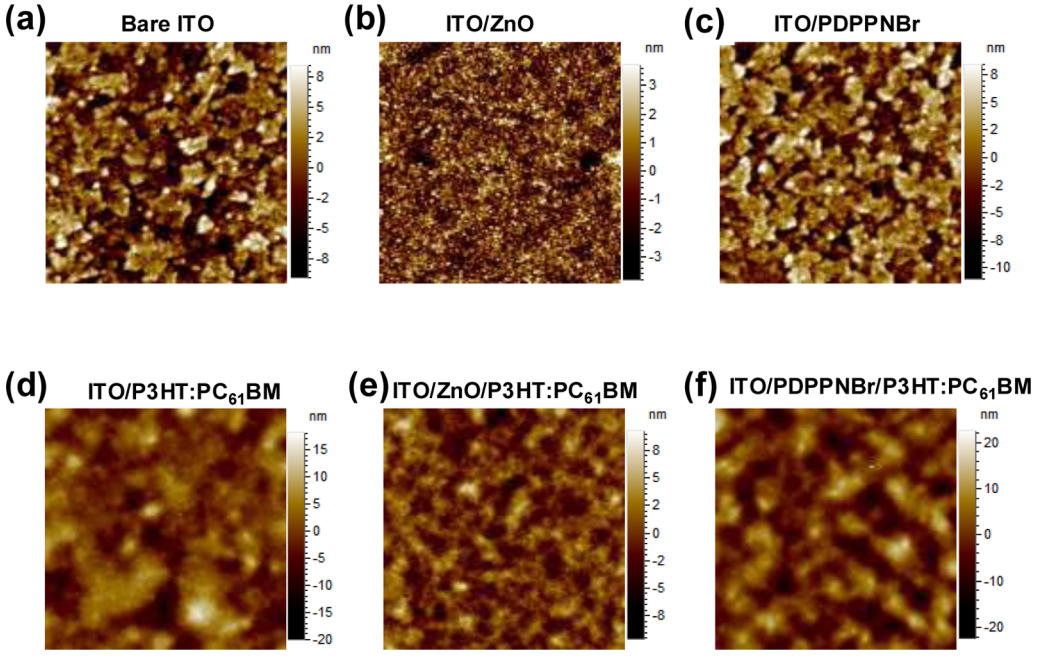


**Figure 3.** AFM morphology images (5 $\mu$m × 5 $\mu$m) of (a) bare ITO, (b) ITO/ZnO, (c) ITO/PDPPNBr, (d) ITO/P3HT:$PC_{61}BM$, (e) ITO/ZnO/P3HT:$PC_{61}BM$, and (f) ITO/ZnO/PDPPNBr/P3HT:$PC_{61}BM$.

In order to further confirm the electronic property variation obtained from the ultraviolet photoelectron spectroscopy, the Kelvin probe method was employed to determine the work function of ITO/PDPPNBr, and result of the commonly efficient



DOI: 10.1021/acs.macromol.5b01137
*Macromolecules* XXXX, XXX, XXX−XXX

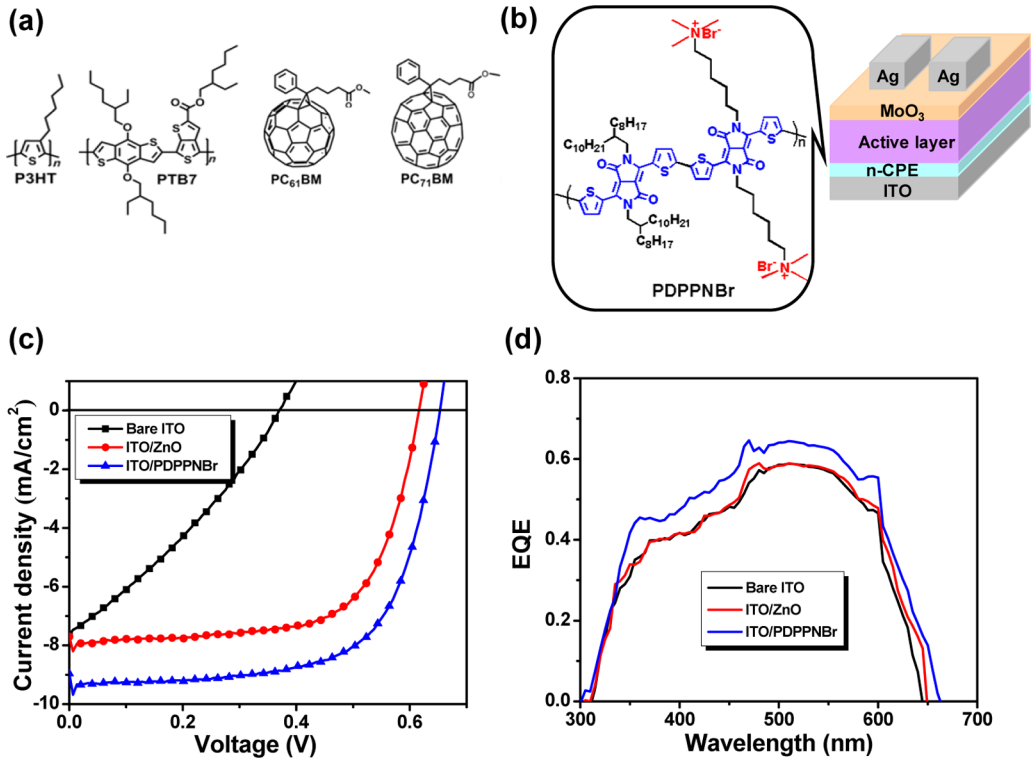


**Figure 4.** (a) Chemical structures of the photoactive layer used in the devices fabrication, (b) structure of the inverted device, (c) the *J*−*V* curves of the PSCs devices ITO/ETLs/P3HT:$PC_{61}BM$/$MoO_3$/Ag with various ETLs, and (d) the corresponding EQE spectra of the PSCs devices with various ETLs.

composite electrode[41] ITO/ZnO (sol−gel ZnO nanoparticles[19] deposited on ITO substrate) was also presented for comparison. Figure 2c demonstrates that the bare ITO and the reference ITO/ZnO exhibit the work function value of −4.70 and −4.41 eV, respectively, in agreement with the literature.[17] Coating a layer of PDPPNBr on ITO leads to a remarkable reduction of WF compared with the bare ITO (−4.25 eV vs −4.70 eV). Note that the WF of ITO/PDPPNBr is even lower than that of ITO/ZnO (−4.25 eV vs −4.41 eV). The reduced WF of ITO/PDPPNBr is very close to the LUMOs of $PC_{61}BM$ and $PC_{71}BM$, which can form an ohmic contact with the active layer and smoothly transport the electrons from fullerene acceptor to the ITO cathode (Figure 2d).

Figure S6 displays the hydrophilic alteration of bare ITO, ITO/ZnO, and ITO/PDPPNBr. The bare ITO exhibits a water contact angle of ca. 73°. After a layer of the so-gel ZnO nanoparticles spin-coated on the ITO, the contact angle to deionized water of ITO/ZnO decreases to ca. 60°. Replacing the ZnO to PDPPNBr leads to the surface of ITO/PDPPNBr with an increased water contact angle of ca. 89°. The more hydrophobic surface of ITO/PDPPNBr again gives a direct proof to verify that the negative bromide counterions tend to locate at the hydrophilic ITO, whereas the hydrophobic conjugated polymer backbone preferentially locates at the side of organic active layer (Figure 2b). The increased hydrophobic surface of ITO/PDPPNBr allows for the more imitated contact with upper active layer. Moreover, the calculated surface energy of ITO/PDPPNBr (30.67 mN/m) is closer to $PC_{61}BM$ and $PC_{71}BM$ (28.1 mN/m) than P3HT (23.8 mN/m), which would be beneficial to a vertical phase separation of the active layer.[42] Additionally, atomic force microscopy (AFM) was also employed to determine the morphology of the bare ITO, ITO/ZnO, and ITO/PDPPNBr. As shown in Figure 3, the bare ITO exhibits a roughness root-mean-square (rms) of 3.29 nm. After being spin-coated with a thin layer ZnO nanoparticles, the surface becomes smoother with a decreased rms of 1.23 nm, while upon deposition of the PDPPNBr on ITO substrate, a relatively rougher surface with a rms of 3.59 nm is obtained. Since the surface wettability and morphology of electrode have been altered by covering a layer of PDPPNBr, it is expected to influence the deposition of the active layer. Thereby, AFM was conducted to investigate the morphology of active layer deposited on bare ITO, ITO/ZnO, and ITO/PDPPNBr. The P3HT:$PC_{61}BM$ active layer was spin-coated on these substrates and then annealed at 150 °C for 10 min. Seen from the images in Figure 3, the P3HT:$PC_{61}BM$ deposited on bare ITO and ITO/ZnO substrates exhibits a roughness rms of 3.1 and 1.8 nm, respectively. It is worthy to note that the PFN, a well-known interlayer for state-of-art PSCs, is not suitable for P3HT:$PC_{61}BM$ devices due to the poor compatibility between interlayer and active layer. Delightfully, deposition of P3HT:$PC_{61}BM$ on the ITO/PDPPNBr develops a robust and uniform film with a roughness rms of 4.3 nm, suggesting a good contact of ITO/PDPPNBr with P3HT:$PC_{61}BM$. The difference in roughness of P3HT:$PC_{61}BM$ is caused from the morphology variation of the substrates. It has been reported a rougher surface of the active layer would facilitate the interfacial adhesion between subsequent hole extraction layer and the active layer; therefore, an improved charge transport can be anticipated.[43,44] In addition, a uniform microphase separation of P3HT:$PC_{61}BM$ is well developed on the ITO/PDPPNBr substrate, which would be very helpful for charge separation and transportation.

To evaluate the interfacial modification function of the novel n-type conjugated polyelectrolyte PDPPNBr as ETL, bulk


DOI: 10.1021/acs.macromol.5b01137
*Macromolecules* XXXX, XXX, XXX−XXX

**Table 1. Device Parameters of the Devices ITO/PDPPNBr/P3HT:$PC_{61}BM$/$MoO_3$/Ag with PDPPNBr Interlayer of Various Thicknesses under the Illumination of AM 1.5G, 100 mW $cm^{-2}$**

| active layer | interlayer (thickness) | $V_{oc}$ (V) | $J_{sc}$ (mA/$cm^2$) | FF (%) | PCE (%) | $R_s$ (Ω $cm^2$) | $R_{sh}$ (Ω $cm^2$) |
|---|---|---|---|---|---|---|---|
| P3HT:$PC_{61}BM$ | | 0.37 | 7.63 | 30.21 | 0.85 | 41.24 | 66.94 |
| | ZnO | 0.62 | 7.70 | 68.03 | 3.25 | 8.90 | 592.48 |
| | PDPPNBr (6 nm) | 0.61 | 7.02 | 67.38 | 2.89 | 1.95 | 2748 |
| | PDPPNBr (12 nm) | 0.65 | 8.95 | 69.29 | 4.03 | 2.14 | 1537 |
| | PDPPNBr (20 nm) | 0.64 | 8.35 | 68.96 | 3.68 | 3.46 | 1665 |
| | PDPPNBr (29 nm) | 0.66 | 7.84 | 65.83 | 3.41 | 13.28 | 1579 |
| PTB7:$PC_{71}BM$ | | 0.46 | 11.67 | 52.8 | 2.83 | 12.26 | 301.42 |
| | ZnO | 0.73 | 14.29 | 68.5 | 7.15 | 4.16 | 2271.55 |
| | PDPPNBr (12 nm) | 0.75 | 15.10 | 70.8 | 8.02 | 2.04 | 2690.82 |

heterojunction (BHJ) solar cells with an inverted structure of ITO/PDPPNBr/active layer/$MoO_3$/Ag were fabricated. The details of the devices fabrication process are provided in the Supporting Information. A schematic device structure and the chemical structures of the active materials employed in this work are shown in Figure 4. First of all, the effect of thickness (6, 12, 20, and 29 nm) of the PDPPNBr on the device performance has been determined, and the optical transmittance spectra of the bare ITO and ITO coated with various thicknesses of PDPPNBr are also investigated. As displayed in Figure S7, the transmittances of ITO/PDPPNBr with different thickness are almost identical to that of the bare ITO, inferring that this n-CPE is suitable as interlayer. Figure 4 shows the illuminated current density−voltage ($J-V$) curves of devices based on P3HT:$PC_{61}BM$ with PDPPNBr as the ETL, and the detailed photovoltaic characteristics are summarized in Table 1. The best PCE of 4.03%, together with an open circuit voltage ($V_{oc}$) of 0.65 V, a short circuit current density ($J_{sc}$) of 8.95 mA/$cm^2$, and a fill factor (FF) of 69.29%, is achieved from the device based on PDPPNBr with an optimized thickness of ∼12 nm (Figure 5a). The device with the ultrathin PDPPNBr cathode interlayer (6 nm) delivers the lowest PCE of 2.9%, presumably due to the incompletely covered interlayer on the ITO electrode. More intriguingly, when the thickness of PDPPNBr increases to 20 and 29 nm, the PCEs of the devices still remain at the high values of 3.68% and 3.41%, respectively. As we all know, most polyelectrolytes (usually based on p-type conjugated or nonconjugated backbone) as interlayers are very sensitive to the thickness, and the thickness limitation is always less than 10 nm. For instance, the optimized thickness of the well-known cathode interlayer PFN is found to be 5−6 nm,[33] and further increasing the interlayer thickness results in a sharply decreased device efficiency. This is because the p-type conjugated or nonconjugated backbone is not beneficial for electron transport; therefore, the electron extraction from active layer to cathode mainly relies on the electron tunneling effect.[45] In order to further confirm this opinion, the control device based nonconjugated polyelectrolyte polyethylenimine ethoxylated (PEIE) ETL was fabricated; the contrastive parameters are shown in Table S2. It is obvious that the PEIE could also tune the interface energy alignment so that a superior $V_{oc}$ was obtained, whereas the inferior $J_{sc}$ was probably caused by the nonconjugated backbone with a poor conductivity. Additionally, increasing the interlayer thickness will inevitably increase the bulk resistance of the interlayer, consequently leading to the sharply decreased electron extraction and transportation. For the PDPPNBr ETL, when the thickness increases from 6 to 29 nm, the series resistance ($R_s$) only slightly increases from 1.95 to 13.28 Ω $cm^2$. To explore the reason behind the unique PDPPNBr ETL, the

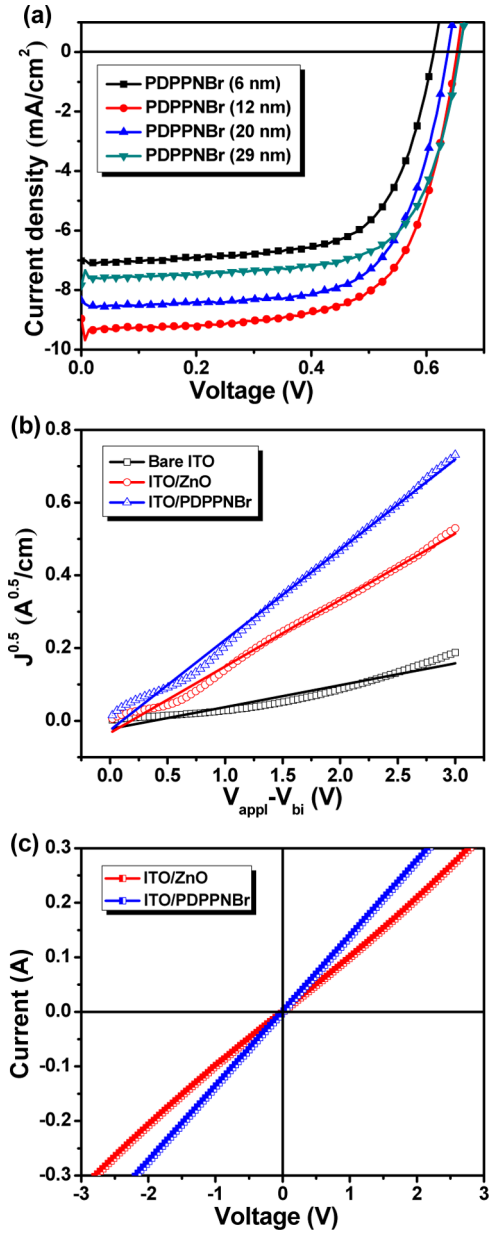


**Figure 5.** (a) $J-V$ characteristics of the devices ITO/PDPPNBr/P3HT:$PC_{61}BM$/$MoO_3$/Ag with PDPPNBr interlayer of various thicknesses under the illumination of AM 1.5G, 100 mW $cm^{-2}$, (b) $J^{0.5}-V$ characteristics of electron-only devices ITO/ETLs/P3HT:$PC_{61}BM$/LiF/Al with different ETLs, and (c) $I-V$ curves for electron-only transfer devices ITO/ETLs/Au.



DOI: 10.1021/acs.macromol.5b01137
*Macromolecules* XXXX, XXX, XXX−XXX

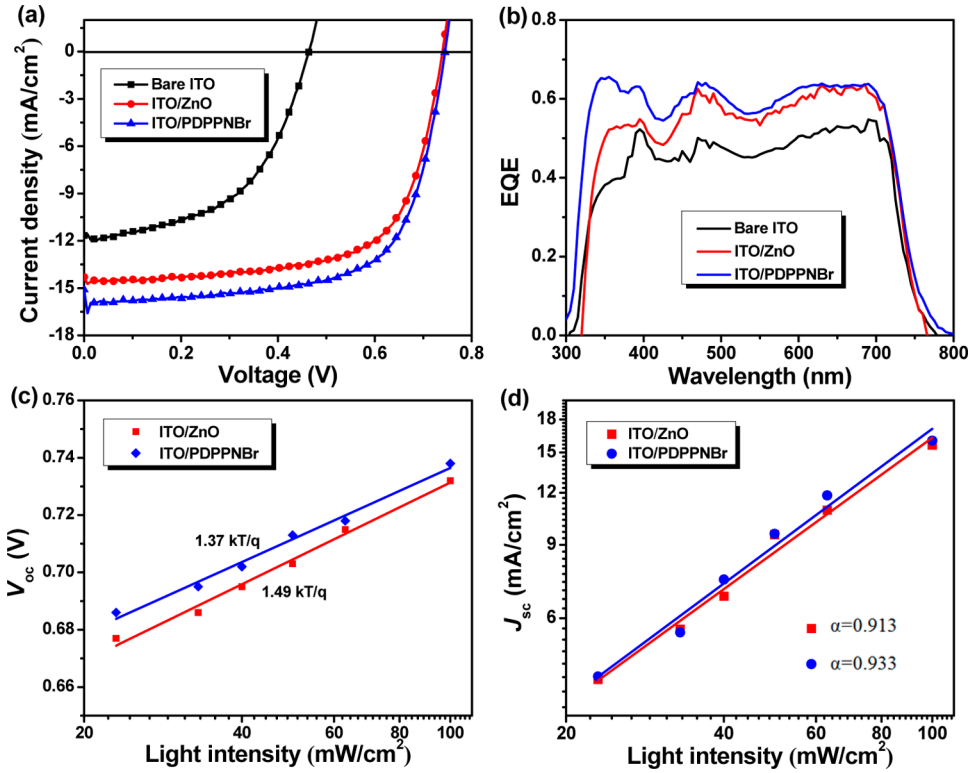


**Figure 6.** (a) $J-V$ curves of the PSCs devices ITO/ETLs/PTB7:$PC_{71}BM$/$MoO_3$/Ag with various ETLs, (b) the corresponding EQE spectra of the PSCs based on PTB7:$PC_{71}BM$ with various ETLs, (c) measured $V_{oc}$ of cells with ZnO and PDPPNBr interlayer plotted against light intensity on a logarithmic scale (symbols), together with linear fits to the data (solid lines), and (d) measured $J_{sc}$ of cells with ZnO and PDPPNBr interlayer plotted against light intensity on a logarithmic scale. Fitting a power law (solid lines) to these data yields $\alpha$. The devices are based on PTB7:$PC_{71}BM$ as active layer.

electron mobility of PDPPNBr in the solar cell devices is estimated using the space-charge limited current (SCLC) method according to the Mott−Gurney equation.[46−48] As plotted in Figure 5b, the device with bare ITO shows an electron mobility of $2.08 \times 10^{-5}$ $cm^2$ $V^{-1}$ $s^{-1}$. After incorporation of PDPPNBr as ETL, the electron mobility is remarkably enhanced to $5.70 \times 10^{-4}$ $cm^2$ $V^{-1}$ $s^{-1}$, which is even higher than that of ZnO ETL ($3.78 \times 10^{-4}$ $cm^2$ $V^{-1}$ $s^{-1}$) (Table S2). In addition, the conductivity of the ZnO and PDPPNBr interlayer was also investigated and compared. As shown in Figure 5c, PDPPNBr displays more superior conductivity over ZnO ($9.98 \times 10^{-6}$ S $cm^{-1}$ vs $7.89 \times 10^{-6}$ S $cm^{-1}$), and its conductivity is even 3 orders of magnitude higher than that of PFN interlayer ($6.9 \times 10^{-9}$ S $cm^{-1}$).[49] The high electron mobility and conductivity of PDPPNBr interlayer mainly originate from the n-type character and the dense packing of planar DPP units, which should be responsible for the highly maintained performance devices with the thick ETL. This novel interlayer could provide the feasibility of large-area roll-to-roll manufacturing techniques.

Superiority of the PDPPNBr ETL can be clearly verified by comparing the devices performances with ITO/PDPPNBr, ITO/ZnO, and bare ITO. From Figure 4 and Table 1 we can see that all of the devices with PDPPNBr ETLs show significantly improved PCE than the control device with bare ITO (0.85%), and PDPPNBr with a thickness of 12, 20, and 29 nm even achieves a higher PCE than the widely used ZnO ETL (3.24%). And the highest efficiency obtained from PDPPNBr (4.03%) shows 374% and 24% improvement over those obtained from bare ITO and ZnO interlayers, respectively. The remarkable improvement in PCE is a result of the overall improved $V_{oc}$ (from 0.37 to 0.65 eV), $J_{sc}$ (from 7.63 to 8.95 mA/$cm^2$), and FF (from 30.2% to 69.3%), suggesting a more favorable charge injection and collection are achieved at the electrodes. The simultaneously increased $V_{oc}$ and $J_{sc}$ values are related to the better energy alignment induced by the dipole moments created from the PDPPNBr with polar groups, which is in good agreement with the UPS and Kelvin probe observation. As revealed by Table 1, compared with bare ITO and ITO/ZnO-based devices, incorporation of PDPPNBr ETL into the device can significantly reduce the series resistance ($R_s$) and increase the shunt resistance ($R_{sh}$), indicating a good interfacial modification to boost charge injection and suppress charge recombination. As a result, a distinctly improved $J_{sc}$ and FF are achieved. Moreover, the desirable morphology of the active layer and favorable interface contact observed from AFM and water contact angle measurement should also account for the $J_{sc}$ and FF enhancement. The highest performance promoted by the PDPPNBr ETL can be further elucidated by the most restrained leakage current in the dark $J-V$ curve (Figure S8). The theoretical $J_{sc}$ obtained by integrating the corresponding external quantum efficiency (EQE) data (in Figure 4d) is also well consistent with the current values from the $J-V$ characteristic.

To further confirm and testify the universality of this novel PDPPNBr ETL, the inverted PSCs devices based on the low-bandgap polymer polythieno[3,4-*b*]-thiophene-*co*-benzodithiophene (PTB7) as a donor and (6,6)-phenyl-$C_{71}$-butyric acid methyl ester ($PC_{71}BM$) as a acceptor were fabricated. The corresponding $J-V$ characteristics and devices parameters are summarized in Figure 6a and Table 1, respectively. As expected, with respect to the bare ITO and ZnO modified ITO electrode,


DOI: 10.1021/acs.macromol.5b01137
*Macromolecules* XXXX, XXX, XXX−XXX

the PDPPNBr modified ITO cathode yields the best PCE as high as 8.02% with a $V_{oc}$ of 0.75 V, a $J_{sc}$ of 15.10, and a FF of 70.8%. Similar to the device with P3HT:$PC_{61}BM$, the notable efficiency of device with PTB7: $PC_{71}BM$ is also mainly attributed to the overall improved device parameter, including $V_{oc}$, $J_{sc}$, and FF. The external quantum efficiency (EQE) curves of the devices are presented in Figure 6b. It can be seen that the PDPPNBr-based device shows the highest EQE value, in accordance with the values obtained from the $J-V$ characteristics in Figure 6a.

Table 1 demonstrates that all of the PDPPNBr-based devices show the dropped $R_s$ and enhanced $R_{sh}$ than the bare ITO and ITO/ZnO-based devices, regardless of the active layer. It can be concluded that incorporation of PDPPNBr ETL into the devices can significantly improve charge injection and suppress charge recombination. To gain deeper insight into the influence of PDPPNBr interlayer on the recombination mechanism in the devices, an additional measurement with respect to the $V_{oc}$ and $J_{sc}$ of the ZnO and PDPPNBr based devices at various light intensities from 23 to 100 mW $cm^{-2}$ was carried out. We plotted $V_{oc}$ versus the logarithm of light intensity following the equation

$$V_{oc} \propto nkT/q \ln(P) \quad (1)$$

where $k$, $T$, $q$, and $P$ are the Boltzmann constant, temperature in kelvin, the elementary charge, and the light intensity, respectively.[50] Fitting the curves in Figure 6c yields a value of $1.49kT/q$ of the cell with ZnO interlayer, while that of cell with PDPPNBr interlayer is $1.37kT/q$, indicating the device with PDPPNBr has less recombination at the interface between the active layer and ITO anode.[51,52] On the other hand, the dependence of $J_{sc}$ upon illumination intensity is plotted on a log–log scale and fitted to a power law according the equation

$$J_{sc} \propto I^{\alpha} \quad (2)$$

where $I$ is the light intensity and $\alpha$ is the exponential factor.[53,54] As shown in Figure 6d, the value $\alpha = 0.913$ and $\alpha = 0.933$ for the PSCs with ZnO and PDPPNBr interlayer, respectively. The result elucidates that the bimolecular recombination is obviously reduced in the device based on PDPPNBr interlayer. The suppressed charge recombination at the interface of active layer and cathode subsequently causes the increase of $J_{sc}$ and FF.

The air stability of polymer solar is also a crucial factor for their practical application; therefore, the air stability of the unencapsulated inverted devices based on P3HT:$PC_{61}BM$ with or without the cathode interlayer was periodically measured for 30 days (Figure 7). Obviously, the device without any cathode buffer layer retained a terrible long-term stability with 28% of its original PCE after being exposed to ambient conditions. In contrast, the device based on PDPPNBr interlayer can still maintained 64% of the initial efficiency after being exposed to ambient conditions for 30 days, which is even higher than the device based on ZnO with 60% of the initial value. The improved long-term stability presumably results from the imitate interface compatibility between the ITO and active layer induced by the novel alcohol conjugated polyelectrolyte.

## 3. CONCLUSIONS

In conclusion, a novel alcohol-soluble conjugated polyelectrolyte PDPPNBr based on n-type backbone is first synthesized and applied as ETL in high performance PSCs. The feature of the conjugated backbone of the polyelectrolyte has significantly impact on the properties. The planar DPP backbone with n-type nature endows the PDPPNBr with high conductivity and

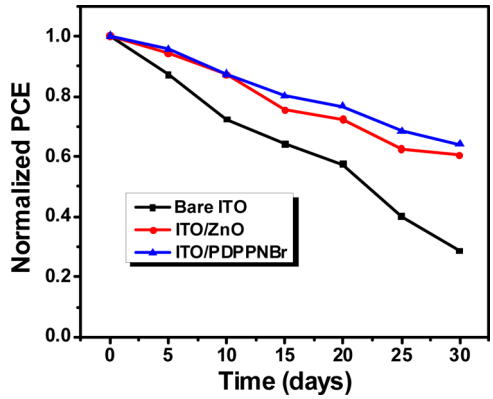


**Figure 7.** Air stability test of the unencapsulated device based P3HT:$PC_{61}BM$ active layer with various electron transport layers for 30 days under ambient conditions.

electron mobility. The interfacial dipole moment created by n-CPE PDPPNBr can substantially reduce the work function of ITO and induce a better energy alignment in the device, facilitating electron extraction and decreasing exctions recombination at active layer/cathode interface. Consequently, the inverted device with n-CPE PDPPNBr as ETL achieves a notable PCE as high as 8.02%. Quite different from the traditional p-type conjugated and nonconjugated polyelectrolytes ETLs, n-CPE PDPPNBr as ETL could function efficiently with a thickness approximate 30 nm, thanks to the high conductivity and electron mobility. The success of PDPPNBr implies that alcohol-soluble n-type conjugated polyelectrolyte could be particularly useful in developing high-performance organic interlayer materials. In addition, though the PDPPNBr would absorb more light with the thickness of the PDPPNBr increase, consequently slightly reduced short circuit current of the devices, the photovoltaic devices still maintained a superior performance due to a desirable conductivity and electron mobility of the novel polyelectrolytes. Therefore, it is instructive for us to design and synthesis the n-CPE interface materials with less light absorption in the future.

## ■ ASSOCIATED CONTENT

### Supporting Information

The Supporting Information is available free of charge on the ACS Publications website at DOI: 10.1021/acs.macromol.5b01137.

Detailed synthesis procedure and corresponding NMR spectra, UV, CV, and molecular orbital diagram of the polymer and polyelectrolyte, and the specific device fabrication and material (PDF)

## ■ AUTHOR INFORMATION

### Corresponding Author

*Tel +86 791 83968703; fax +86 791 83968830; e-mail chenlie@ncu.edu.cn (L.C.).

### Notes

The authors declare no competing financial interest.

## ■ ACKNOWLEDGMENTS

This work was financially supported by the National Science Fund for Distinguished Young Scholars (51425304), National Natural Science Foundation of China (51263016, 51473075 and 21402080), National Basic Research Program of China (973



DOI: 10.1021/acs.macromol.5b01137
*Macromolecules* XXXX, XXX, XXX–XXX

Program 2014CB260409), and Graduate Innovation Fund Projects of Jiangxi Province (YC2014-S041).

## REFERENCES


(1) Thompson, B. C.; Frechet, J. M. *Angew. Chem., Int. Ed.* **2008**, *47*, 58−77.
(2) Cheng, Y.-J.; Yang, S.-H.; Hsu, C.-S. *Chem. Rev.* **2009**, *109*, 5868−5923.
(3) Beaujuge, P. M.; Frechet, J. M. *J. Am. Chem. Soc.* **2011**, *133*, 20009−29.
(4) Chen, Y. C.; Hsu, C. Y.; Lin, R. Y.; Ho, K. C.; Lin, J. T. *ChemSusChem* **2013**, *6*, 20−35.
(5) Wong, W.-Y.; Ho, C.-L. *Acc. Chem. Res.* **2010**, *43*, 1246−1256.
(6) Liu, Y.; Zhao, J.; Li, Z.; Mu, C.; Ma, W.; Hu, H.; Jiang, K.; Lin, H.; Ade, H.; Yan, H. *Nat. Commun.* **2014**, *5*, 5293.
(7) You, J.; Dou, L.; Yoshimura, K.; Kato, T.; Ohya, K.; Moriarty, T.; Emery, K.; Chen, C. C.; Gao, J.; Li, G.; Yang, Y. *Nat. Commun.* **2013**, *4*, 1446.
(8) Chen, J.-D.; Cui, C.; Li, Y.-Q.; Zhou, L.; Ou, Q.-D.; Li, C.; Li, Y.; Tang, J.-X. *Adv. Mater.* **2015**, *27*, 1035−1041.
(9) He, Z.; Xiao, B.; Liu, F.; Wu, H.; Yang, Y.; Xiao, S.; Wang, C.; Russell, T. P.; Cao, Y. *Nat. Photonics* **2015**, *9*, 174−179.
(10) Cui, C.; Wong, W.-Y.; Li, Y. *Energy Environ. Sci.* **2014**, *7*, 2276−2284.
(11) He, Z.; Zhong, C.; Huang, X.; Wong, W. Y.; Wu, H.; Chen, L.; Su, S.; Cao, Y. *Adv. Mater.* **2011**, *23*, 4636−43.
(12) Hau, S. K.; Yip, H.-L.; Baek, N. S.; Zou, J.; O'Malley, K.; Jen, A. K. Y. *Appl. Phys. Lett.* **2008**, *92*, 253301.
(13) Kao, C.-S.; Chen, F.-C.; Liao, C.-W.; Huang, M. H.; Hsu, C.-S. *Appl. Phys. Lett.* **2012**, *101*, 193902.
(14) He, Z.; Zhong, C.; Su, S.; Xu, M.; Wu, H.; Cao, Y. *Nat. Photonics* **2012**, *6*, 591−595.
(15) Zou, J.; Yip, H.-L.; Zhang, Y.; Gao, Y.; Chien, S.-C.; O'Malley, K.; Chueh, C.-C.; Chen, H.; Jen, A. K. Y. *Adv. Funct. Mater.* **2012**, *22*, 2804−2811.
(16) Kyaw, A. K.; Wang, D. H.; Gupta, V.; Zhang, J.; Chand, S.; Bazan, G. C.; Heeger, A. J. *Adv. Mater.* **2013**, *25*, 2397−402.
(17) Yip, H.-L.; Jen, A. K. Y. *Energy Environ. Sci.* **2012**, *5*, 5994.
(18) Duan, C.; Zhang, K.; Zhong, C.; Huang, F.; Cao, Y. *Chem. Soc. Rev.* **2013**, *42*, 9071−104.
(19) Sun, Y.; Seo, J. H.; Takacs, C. J.; Seifter, J.; Heeger, A. J. *Adv. Mater.* **2011**, *23*, 1679−83.
(20) Liao, H.-C.; Lee, C.-H.; Ho, Y.-C.; Jao, M.-H.; Tsai, C.-M.; Chuang, C.-M.; Shyue, J.-J.; Chen, Y.-F.; Su, W.-F. *J. Mater. Chem.* **2012**, *22*, 10589.
(21) Zhang, Z.-G.; Li, H.; Qi, B.; Chi, D.; Jin, Z.; Qi, Z.; Hou, J.; Li, Y.; Wang, J. *J. Mater. Chem. A* **2013**, *1*, 9624.
(22) Reilly, T. H.; Hains, A. W.; Chen, H.-Y.; Gregg, B. A. *Adv. Energy Mater.* **2012**, *2*, 455−460.
(23) Zhou, Y.; Fuentes-Hernandez, C.; Shim, J.; Meyer, J.; Giordano, A. J.; Li, H.; Winget, P.; Papadopoulos, T.; Cheun, H.; Kim, J.; Fenoll, M.; Dindar, A.; Haske, W.; Najafabadi, E.; Khan, T. M.; Sojoudi, H.; Barlow, S.; Graham, S.; Bredas, J. L.; Marder, S. R.; Kahn, A.; Kippelen, B. *Science* **2012**, *336*, 327−32.
(24) Guan, X.; Zhang, K.; Huang, F.; Bazan, G. C.; Cao, Y. *Adv. Funct. Mater.* **2012**, *22*, 2846−2854.
(25) Meng, B.; Fu, Y.; Xie, Z.; Liu, J.; Wang, L. *Macromolecules* **2014**, *47*, 6246−6251.
(26) Zheng, Z.; Zhang, S.; Zhang, M.; Zhao, K.; Ye, L.; Chen, Y.; Yang, B.; Hou, J. *Adv. Mater.* **2015**, *27*, 1189−1194.
(27) Tordera, D.; Kuik, M.; Rengert, Z. D.; Bandiello, E.; Bolink, H. J.; Bazan, G. C.; Nguyen, T. Q. *J. Am. Chem. Soc.* **2014**, *136*, 8500−3.
(28) Mai, C. K.; Schlitz, R. A.; Su, G. M.; Spitzer, D.; Wang, X.; Fronk, S. L.; Cahill, D. G.; Chabinyc, M. L.; Bazan, G. C. *J. Am. Chem. Soc.* **2014**, *136*, 13478−81.
(29) Seo, J. H.; Gutacker, A.; Sun, Y.; Wu, H.; Huang, F.; Cao, Y.; Scherf, U.; Heeger, A. J.; Bazan, G. C. *J. Am. Chem. Soc.* **2011**, *133*, 8416−9.
(30) Sun, J.; Zhu, Y.; Xu, X.; Lan, L.; Zhang, L.; Cai, P.; Chen, J.; Peng, J.; Cao, Y. *J. Phys. Chem. C* **2012**, *116*, 14188−14198.
(31) Li, Y.-L.; Cheng, Y.-S.; Yeh, P.-N.; Liao, S.-H.; Chen, S.-A. *Adv. Funct. Mater.* **2014**, *24*, 6811−6817.
(32) Kang, H.; Hong, S.; Lee, J.; Lee, K. *Adv. Mater.* **2012**, *24*, 3005−9.
(33) Zhang, Z.-G.; Qi, B.; Jin, Z.; Chi, D.; Qi, Z.; Li, Y.; Wang, J. *Energy Environ. Sci.* **2014**, *7*, 1966.
(34) Liu, S.; Zhang, K.; Lu, J.; Zhang, J.; Yip, H. L.; Huang, F.; Cao, Y. *J. Am. Chem. Soc.* **2013**, *135*, 15326−9.
(35) Liu, Q.; Ho, C.-L.; Lo, Y. H.; Li, H.; Wong, W.-Y. *J. Inorg. Organomet. Polym. Mater.* **2015**, *25*, 159−168.
(36) Xie, C.; Chen, L.; Chen, Y. *J. Phys. Chem. C* **2013**, *117*, 24804−24814.
(37) Osaka, I.; Sauvé, G.; Zhang, R.; Kowalewski, T.; McCullough, R. D. *Adv. Mater.* **2007**, *19*, 4160−4165.
(38) Kanimozhi, C.; Yaacobi-Gross, N.; Chou, K. W.; Amassian, A.; Anthopoulos, T. D.; Patil, S. *J. Am. Chem. Soc.* **2012**, *134*, 16532−5.
(39) Kang, R.; Oh, S. H.; Kim, D. Y. *ACS Appl. Mater. Interfaces* **2014**, *6*, 6227−36.
(40) Choi, H.; Park, J. S.; Jeong, E.; Kim, G. H.; Lee, B. R.; Kim, S. O.; Song, M. H.; Woo, H. Y.; Kim, J. Y. *Adv. Mater.* **2011**, *23*, 2759−63.
(41) Chen, L.; Xie, C.; Chen, Y. *Macromolecules* **2014**, *47*, 1623−1632.
(42) Ma, D.; Lv, M.; Lei, M.; Zhu, J.; Wang, H.; Chen, X. *ACS Nano* **2014**, *8*, 1601−1608.
(43) Ma, W.; Yang, C.; Gong, X.; Lee, K.; Heeger, A. J. *Adv. Funct. Mater.* **2005**, *15*, 1617−1622.
(44) Sekine, N.; Chou, C.-H.; Kwan, W. L.; Yang, Y. *Org. Electron.* **2009**, *10*, 1473−1477.
(45) Braun, S.; Salaneck, W. R.; Fahlman, M. *Adv. Mater.* **2009**, *21*, 1450−1472.
(46) Liu, Y.; Wan, X.; Wang, F.; Zhou, J.; Long, G.; Tian, J.; Chen, Y. *Adv. Mater.* **2011**, *23*, 5387−91.
(47) Cheng, Y.-J.; Hsieh, C.-H.; Li, P.-J.; Hsu, C.-S. *Adv. Funct. Mater.* **2011**, *21*, 1723−1732.
(48) Zhao, G.; He, Y.; Xu, Z.; Hou, J.; Zhang, M.; Min, J.; Chen, H.-Y.; Ye, M.; Hong, Z.; Yang, Y.; Li, Y. *Adv. Funct. Mater.* **2010**, *20*, 1480−1487.
(49) Woo Lee, H.; Young, O. J.; Il Lee, T.; Soon Jang, W.; Bum Yoo, Y.; Sang Chae, S.; Ho Park, J.; Min Myoung, J.; Moon Song, K.; Koo Baik, H. *Appl. Phys. Lett.* **2013**, *102*, 193903.
(50) Koster, L. J. A.; Mihailetchi, V. D.; Ramaker, R.; Blom, P. W. *Appl. Phys. Lett.* **2005**, *86*, 123509−123509−3.
(51) Choi, H.; Kim, H. B.; Ko, S. J.; Kim, J. Y.; Heeger, A. J. *Adv. Mater.* **2015**, *27*, 892−6.
(52) Jiang, Y.; Yang, M.; Huang, X.; Gao, J.; Zhan, C.; Xiao, S. *Polym. Chem.* **2015**, *6*, 1383−1392.
(53) Cowan, S. R.; Roy, A.; Heeger, A. J. *Phys. Rev. B: Condens. Matter Mater. Phys.* **2010**, *82*, 245207.
(54) Kyaw, A. K.; Wang, D. H.; Wynands, D.; Zhang, J.; Nguyen, T. Q.; Bazan, G. C.; Heeger, A. J. *Nano Lett.* **2013**, *13*, 3796−801.




DOI: 10.1021/acs.macromol.5b01137
*Macromolecules* XXXX, XXX, XXX−XXX